Inorg. Chem. **2002**, *41*, 2250–2259

Ru^{II} Electron Transfer Systems Containing S-Donor Ligands

Cordélia S. Araújo,[†] Michael G. B. Drew,[‡] Vítor Félix,*[,†] Lorna Jack,[§] João Madureira,[†] Mike Newell,[||] Sue Roche,[||] Teresa M. Santos,[†] Jim A. Thomas,*[,||] and Lesley Yellowlees*[,§]

University of Aveiro, 3810-193 Aveiro, Portugal, Department of Chemistry, The University, Whiteknights, Reading RG6 6AD, UK, Department of Chemistry, Joseph Black Building, West Mains Road, Edinburgh, Scotland EH9 3JJ, UK, Department of Chemistry, Dainton Building, University of Sheffield, Brook Hill, Sheffield S3 7HF, UK

Received August 20, 2001

The synthesis and properties of 3 new ligand-bridged bimetallic complexes, $\mathbf{1}^{2+}$, $\mathbf{2}^{2+}$, and $\mathbf{3}^{2+}$, containing $[RuCl([9]aneS_3)]^+$ metal centers are reported. Each complex was bridged by a different ditopic ligand. $\mathbf{1}^{2+}$ is bridged by 3,6-bis(2-pyridyl)-1,2,4,5-tetrazine (bptz), while $\mathbf{2}^{2+}$ and $\mathbf{3}^{2+}$ are bridged by 2,3-bis(2-pyridyl)pyrazine (dpp) and 2,2′-bipyrimidine (bpym), respectively. The $Ru^{[II]}$ isovalent states of these complexes have been investigated using a variety of techniques. In the case of $\mathbf{3}^{2+}$, X-ray crystallography studies show preferential crystallization of an anti form with respect to coordinated chloride ligands (crystal data for $[\mathbf{3}][Cl_2]\cdot 4H_2O$: $C_{20}H_{38}Cl_4N_4O_4Ru_2S_6$, monoclinic, space group $P2_1/a$, $a = 10.929(14)$, $b = 13.514(17)$, $c = 11.299(16)$ Å, $\beta = 90.52(1)$, $V = 1669$ Å^3, $Z = 2$). UV/vis spectroscopy shows that spectra of these complexes are dominated by intraligand ($\pi\rightarrow\pi^*$) and metal-to-ligand Ru(d)→L(π^*) charge transfer transitions. Electrochemical studies reveal that metal–metal interactions are sufficiently intense to generate the Ru^{III}/Ru^{II} mixed valence $[\{RuCl([9]aneS_3)_2\}(L–L)]^{3+}$ state, where L–L = individual bridging ligands. Although the $\mathbf{1}^{3+}$, $\mathbf{2}^{3+}$, and $\mathbf{3}^{3+}$ mixed valence states were EPR silent at room temperature and 77 K, isotropic solution spectra were observed for the electrochemically generated radical cations $\mathbf{1}^+$, $\mathbf{2}^+$, and $\mathbf{3}^+$, with $\mathbf{1}^+$ displaying well-resolved hyperfine coupling to bridging ligand nitrogens. Using UV/vis/NIR spectroelectrochemistry, we investigated optical properties of the mixed valence complexes. All three showed intervalence charge transfer (IVCT) bands that are much more intense than electrochemical data indicate. Indeed, a comparison of IVCT data for $\mathbf{1}^{3+}$ with an analogous structure containing $[(NH3)_3Ru]^{2+}$ metal centers shows that the IVCT in the new complex is an order of magnitude more intense. It is concluded that although the new complexes show relatively weak electrostatic interactions, they possess large resonance energies.

Introduction

Electron transfer (ET) processes are vital to biological systems. Organelles such as mitochondria and chloroplasts are the energy conversion apparatus of eukaryotic cells. In these structures, electron transfer is used to drive cellular metabolism[1] and photosynthesis,[2] respectively. A great deal of insight into electron transfer processes has been drawn from relatively simple synthetic models. For example, the Marcus theory prediction of an inverted region for ET was confirmed by such experimental studies.[3] A particularly rich area for such research is based on studies of mixed valence coordination complexes.

Mixed valence coordination chemistry has been dominated for some time by ruthenium (II/III) complexes,[4] most of them being modeled on the Creutz−Taube (CT) ion.[5] Such systems have also played an important role in the development of

* To whom correspondence should be addressed. E-mail (J.A.T.): james.thomas@sheffield.ac.uk.
[†] University of Aveiro. E-mail: vfelix@dq.ua.pt (V.F.).
[‡] The University, Whiteknights. Fax: +44 (0)118 931-8453. E-mail: m.g.b.drew@reading.ac.uk (M.G.B.D.).
[§] Joseph Black Building. Fax: +44 (0)131 650 7341. E-mail: L.j.yellowlees@ed.ac.uk (L.Y.).
[||] University of Sheffield. Fax: +44 (0)114 273 8673.

(1) Hatefi, Y. *Annu. Rev. Biochem*. **1985**, *54*, 1015.
(2) Barber, J.; Andersson, B. *Nature* **1994**, *370*, 31.
(3) See, for example: Miller, J. R.; Calcaterra, L. T.; Closs, G. L. *J. Am. Chem. Soc.* **1984**, *106*, 3047.
(4) See, for example: (a) Richardson, D. E.; Taube, H. *Coord. Chem. Rev.* **1984**, *60*, 107. (b) Juris, A.; Balzani, V.; Barigelletti, F.; Capagna, S.; Belser, P.; von Zelewsky, A. *Coord. Chem. Rev.* **1988**, *84*, 85. (c) Kaim, W.; Klein, A.; Glöckle, M. *Acc. Chem. Res.* **2000**, *33*, 755.
(5) (a) Creutz, C.; Taube, H. *J. Am. Chem. Soc.* **1969**, *91*, 3988. (b) Creutz, C.; Taube, H. *J. Am. Chem. Soc*. **1973**, *95*, 1086. (c) Hush, N. S. *Prog. Inorg. Chem.* **1967**, *8*, 391. (d) Creutz, C. *Prog. Inorg. Chem.* **1983**, *30*, 1. (e) Crutchley, R. J. *Adv. Inorg. Chem.* **1994**, *41*, 273.

10.1021/ic010882i CCC: $22.00
Published on Web 03/26/2002

devices for molecular electronics,[6] where they have formed the basic components of molecular wires and molecular switches. The goal of such research is to develop systems displaying electronic communication between metal centers and, thus, long-range electron transfer and photoinduced charge separation.[7] So far, research has involved changing the bridging ligands[5d,e,8] and the metal ion.[9] However, despite previous research revealing that the ET properties of such systems are highly dependent on the nature of the metal center, virtually all these complexes contain nitrogen-based ligands such as NH_3 and 2,2′-bipyridine (bpy) coordinated to the metal ion.

Our aim has been to broaden the experimental basis of mixed valence chemistry, by introducing new metal organic fragments containing sulfur-donor ligands. Such ligands are particularly pertinent as many biological ET systems are based on transition metals coordinated to S-donor sites.[10]

Previous work in our laboratories has demonstrated that incorporation of such thiacrown ligands into monometallic systems clearly modulates their chemical and physical properties relative to more conventional N-donor complexes.[11] Furthermore, a preliminary report[12] has demonstrated that a bimetallic complex containing $[RuCl([9]aneS_3)]^+$ metal centers behaves as a strongly interacting Robin and Day[13] Class III system. Here we report a more detailed study on this complex and related systems that indicate that the chemical and ET properties of these new complexes diverge from those of previously studied systems. In particular, these new systems display more intense intermetallic interactions than would be expected from electrochemical studies alone.

Results

An ideal starting material for complexes that incorporate $[9]aneS_3$ is the previously reported $[Ru(DMSO)Cl_2([9]aneS_3)]$.[14] The bridging ligands chosen for this initial study were either commercially available (2,2′-bipyrimidine (bpym), 2,3-bis(2-pyridyl)pyrazine (dpp)) or readily synthesized (3,6-bis(2-pyridyl)-1,2,4,5-tetrazine (bptz)).[15]

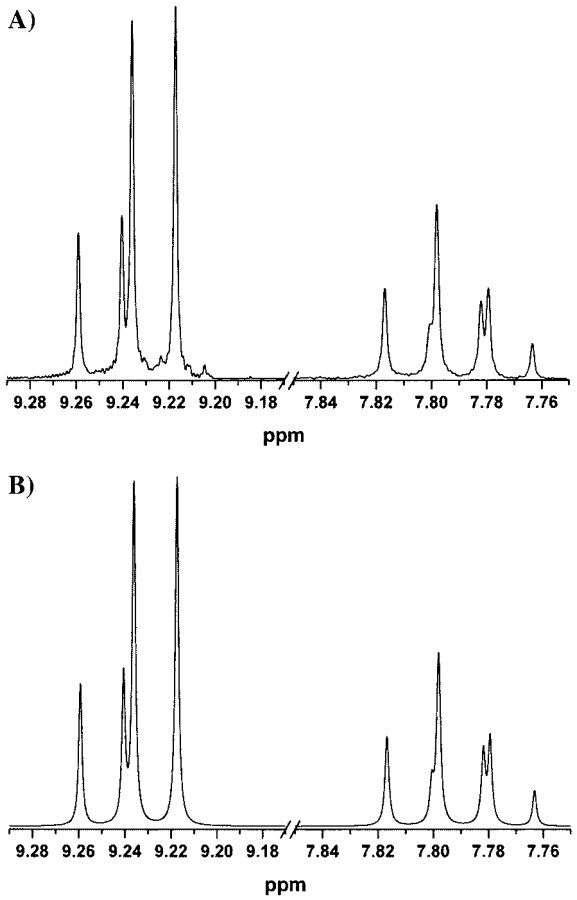

Figure 1. ^1H NMR aromatic region of $\mathbf{3}^{2+}$ in CD_3CN. Two isomers are present with a 1:2.4 ratio; major anti form 9.227 (d, 4H), 7.798 (t, 2H; $J = 5.7$) and minor syn form 9.250 (d, 4H), 7.782 (t, 2H; $J = 5.7$); (A) experimental and (B) calculated pattern (software used, MestRe-C V.2.3.3; spectrometer frequency, 300.13 MHz; apodization, sine squared, 60°; Fourier transform, 131072 points).

Bimetallic complexes of all three ligands can be prepared by reacting $[Ru(DMSO)Cl_2([9]aneS_3)]$ with the relevant ligand in a 2:1 ratio (see below).

The products were isolated as hexafluorophosphate salts. $\mathbf{3}^{2+}$ proved to be sufficiently pure to require no further workup, while analytically pure samples of $\mathbf{1}^{2+}$ and $\mathbf{2}^{2+}$ were obtained by column chromatography.

All the complexes were characterized by ^1H NMR, FAB or ES-MS, and elemental analysis. Additionally, $\mathbf{3}^{2+}$ was further characterized by X-ray crystallography studies.

Structural Studies: ^1H NMR. In any bimetallic complex containing $[RuCl([9]aneS_3)]^+$ metal centers, two possible isomers may be formed, with the chlorides taking syn or anti positions. NMR studies on $\mathbf{1}^{2+}$, $\mathbf{2}^{2+}$, and $\mathbf{3}^{2+}$ clearly indicate both forms in solution, although only one of these structures predominates. From modeling studies, it is clear that the anti isomer is preferentially formed. For example, for $\mathbf{3}^{2+}$, software models confirm that the syn:anti ratio is

(6) (a) Astruc, D. *Acc. Chem. Res*. **1997**, *30*, 383. (b) Ward, M. D. *Chem. Soc. Rev*. **1995**, *24*, 121.
(7) Fox, M. A. *Acc. Chem. Res*. **1999**, *32*, 201.
(8) See, for example: (a) Balzani, V.; Scandola, F. *Pure Appl. Chem.* **1990**, *8*, 1457. (b) Haga, M.; Ano, T.; Kano, K.; Yamabe, S. *Inorg. Chem.* **1991**, *30*, 3843. (c) Aquino, M. A. S.; Lee, F. L.; Gabe, E. J.; Bensimon, C.; Greedau, J. E.; Crutchley, R. J. *J. Am. Chem. Soc.* **1992**, *114*, 5130.
(9) (a) Denti, G.; Campagna, S.; Serroni, S.; Ciano, M.; Balzani, V. *J. Am. Chem. Soc.* **1992**, *114*, 2944. (b) Serroni, S.; Denti, G. *Inorg. Chem.* **1992**, *32*, 4251. (c) Bruns, W.; Kaim, W.; Waldhör, E.; Krejcik, M. *J. Chem. Soc, Chem. Commun.* **1993**, 1868. (d) Strouse, G. F.; Schoonover, J. R.; Duesing, R.; Meyer, T. J. *Inorg. Chem.* **1995**, *34*, 2725.
(10) (a) *Iron*−*Sulfur Proteins*; Spiro, T. G., Ed.; Wiley-Interscience: New York, 1982. (b) Soloman, E. I.; Brunold, T. C.; Davies, M. I.; Kemsley, J. N.; Lee, S.-K.; Lehnert, N.; Neese, F.; Skulan, A. J.; Yang, Y.-S.; Zhou, J. *Chem. Rev.* **2000**, *100*, 235.
(11) (a) Roche, S.; Adams, H.; Spey, S. E.; Thomas, J. A. *Inorg. Chem.* **2000**, *39*, 2385. (b) Santos, T. M.; Goodfellow, B. J.; Madureira, J.; Pedrosa de Jesus, J.; Félix, V.; Drew, M. G. B. *New J. Chem.* **1999**, *23*, 1015. (c) Madureira, J.; Santos, T. M.; Goodfellow, B. J.; Pedrosa de Jesus, M. J.; Santana-Marques, M. G.; Drew, M. G. B.; Félix, V. *J. Chem. Soc., Dalton Trans.* **2000**, 4422.
(12) Roche, S.; Yellowlees, L. J.; Thomas, J. A. *Chem. Commun.* **1998**, 1429.
(13) Robin, M. B.; Day, P. *Adv. Inorg. Chem. Radiochem.* **1967**, *10*, 247.
(14) Landgrafe, C.; Sheldrick, W. S. *J. Chem. Soc., Dalton Trans.* **1994**, 1885.
(15) (a) Libman, D. D.; Slack, R. *J. Chem. Soc.* **1956**, 2253. (b) Geldard, J. F.; Lions, F. *J. Org. Chem*. **1965**, *30*, 318.

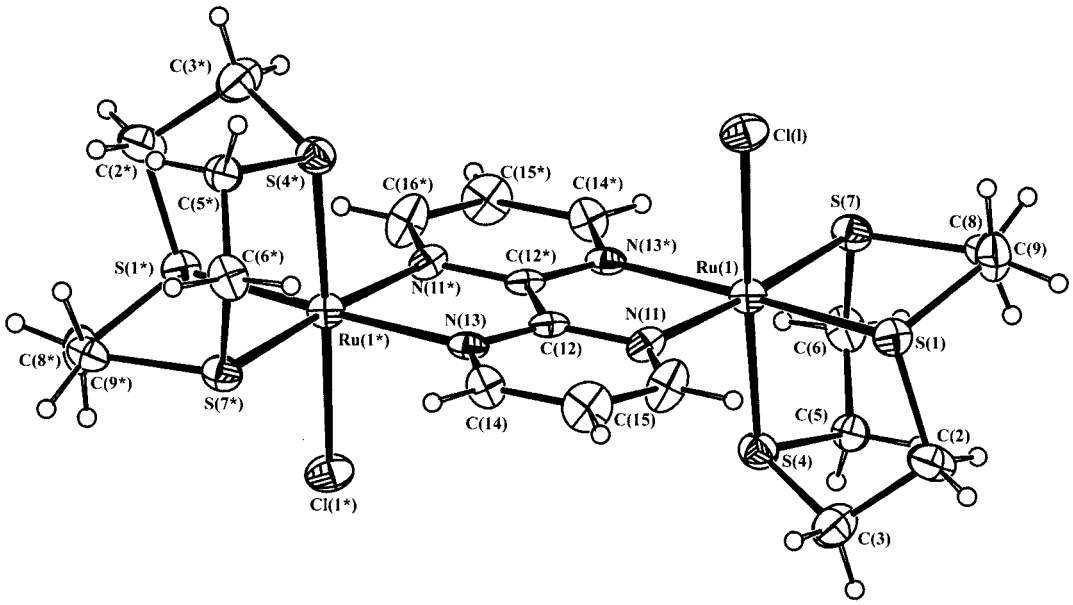

Figure 2. An ORTEP view of the molecular structure of [**3**][Cl_2] with the labeling scheme adopted; thermal ellipsoids are drawn at the 30% probability level.

Table 1. Bond Lengths (Å) and Angles (deg) in the Ru(II) Coordination Sphere of **3**

Ru(1)−N(11)	2.120(11)	Ru(1)−N(13*)[a]	2.116(12)
Ru(1)−S(1)	2.306(5)	Ru(1)−S(4)	2.286(5)
Ru(1)−S(7)	2.317(4)	Ru(1)−Cl(1)	2.424(4)
N(11)−Ru(1)−N(13*)	78.4(4)	N(11)−Ru(1)−S(4)	94.6(3)
N(13*)−Ru(1)−S(4)	93.7(3)	N(13*)−Ru(1)−S(1)	173.8(3)
S(4)−Ru(1)−S(1)	88.2(2)	N(11)−Ru(1)−S(7)	176.1(4)
N(13*)−Ru(1)−S(7)	98.4(4)	S(4)−Ru(1)−S(7)	87.9(2)
S(1)−Ru(1)−S(7)	87.5(2)	N(11)−Ru(1)−Cl(1)	85.9(3)
N(13*)−Ru(1)−Cl(1	88.9(3)	S(4)−Ru(1)−Cl(1)	177.4(2)
S(1)−Ru(1)−Cl(1)	89.2(2)	S(7)−Ru(1)−Cl(1)	91.7(2)

[a] The * denotes the symmetry operation $1 - x + 2, -y + 2, -z + 1$.

1:2.4 (Figure 1). Presumably, the anti form is favored due to the presence of less unfavorable steric interactions in this structure relative to that in the syn isomer. Certainly, crystallography studies on $\mathbf{3}^{2+}$ show that the anti isomer preferentially crystallizes (vide infra).

X-ray Crystallography. The solid-state structure of the PF_6^- salt of the mononuclear complex $\mathbf{4}^+$ has been reported in previous work.[11b]

Here, we present the X-ray determination of the hydrated Cl^- salt of the binuclear cationic complex $\mathbf{3}^{2+}$. Several of the investigated crystals showed rough shapes that easily crumbled. These crystals displayed weak diffraction patterns with roughly defined spots, suggesting a twin crystal. This was confirmed during the structure refinement process. Nevertheless, the collected diffraction data allowed the unequivocal determination of the solid structure. The unit cell contains two centrosymmetric complex cations $\mathbf{3}^{2+}$, eight water molecules, and four chloride anions leading to the molecular formula $[\{Ru([9]aneS_3)Cl\}_2(bpym)]Cl_2 \cdot 4H_2O$.

The molecular structure of $\mathbf{3}^{2+}$ together with the atomic notation adopted is shown in Figure 2. Bond lengths and angles at the Ru(II) center are given in Table 1.

Two {Ru([9]aneS$_3$)Cl} moieties are linked by a bpym bridge in a centrosymmetric crystallographic arrangement. Each ruthenium(II) center exhibits a distorted octahedral geometry with the equatorial plane determined by two nitrogen atoms of the bpym ligand and two sulfurs from the macrocyclic ligand [9]aneS$_3$. Full coordination is achieved with the remaining sulfur and a chlorine atom. The equivalent geometric arrangement with similar dimensions was found for mononuclear complex $\mathbf{4}^+$. In fact, the metal coordination spheres for these two complexes match very closely, giving root-mean-square deviations (RMS) in the atomic positions of only 0.038 Å. In both cases, the Ru−S axial bonds are slightly shorter than the equatorial Ru−S bonds due to the different trans influence of the chlorine and the polypyridyl ligands. The chelating N−Ru−N angle of 78.4(4)° in $\mathbf{3}^{2+}$ and 77.9(2)° in $\mathbf{4}^+$ reflects the small bite angle of bpym and represents the most significant angle deviation from an ideal octahedral coordination sphere. In addition, the Ru−N, Ru−S, and Ru−Cl distances correlate well with previously published X-ray data for structures of related Ru^{II}[9]aneS$_3$ polypyridylic systems.[11c]

However, some structural differences between $\mathbf{3}^{2+}$ and $\mathbf{4}^+$ are observed. In particular, while the macrocycle [9]aneS$_3$ adopts typical *fac*-coordination in both complexes, different conformations were found. The complex $\mathbf{4}^+$ has a mirror crystallographic plane, and the macrocycle displays an unusual conformation with C_s symmetry; in the complex $\mathbf{3}^{2+}$, the macrocycle is facially coordinated via a conformation that has been found in many metal transition complexes.[16] It is interesting to note that while a molecular mechanics and dynamics study in the gas phase gave 13 conformations with energies between 4.5 and 8.3 kcal/mol, this latter conformation has the lowest energy.[17] Furthermore, it is also the conformation of the free macrocycle in the solid state.[18]

A large number of X-ray structures of binuclear complexes containing bpym bridging two metal transition centers are

(16) Allen, F. H.; Davies, J. E.; Galloy, J. J.; Johnson, O.; Kennard, O.; Macrae, C. F.; Mitchell, E. M.; Mitchel, G. F.; Smith, D. J. M.; Watson, G. *J. Chem. Inf. Comput. Sci.* **1991**, *31*, 187.

now available from the Cambridge Data Base.[16] However, the Ru(μ-bpym)Ru bridging system seems to be rare and only one example was found, i.e., the complex *meso*-($\Lambda\Delta$)-[{Ru(dmbpy)$_2$}$_2$(μ-bpym)]$^{4+}$ (dmbpy = 4,4′-dimethyl-2,2′-bipyridine), in which two Ru(dmbpy)$_2$ moieties are connected by a bpym bridge in a distorted octahedral geometric arrangement.[19] Its structure also contains a crystallographic inversion center. In complex **3**$^{2+}$, the bpym bridge holds the two ruthenium centers at an intermolecular distance of 5.705(6) Å, which is longer than the 5.559 Å observed for *meso*-($\Lambda\Delta$)-[{Ru(dmbpy)$_2$}$_2$(μ-bpym)]$^{4+}$. Although these two distances are within the typical range of the metal−metal distances found for M(μ-bpym)M systems, that is, 5.370−6.247 Å, larger separations have been reported: for example, a recently described mercury complex had a Hg···Hg distance of 7.012 Å.[20] These data show that bpym has the capability to bridge metal centers with very different stereoelectronic properties. Furthermore, bpym is able to hold two metal centers at intermetallic distances comparable to those found for complexes containing dpp (6.779−7.026 Å) (CSD) and bptz bridges (6.742 Å) (CSD).

When the crystal packing of complex **3**$^{2+}$ is viewed perpendicular to the [011] crystallographic plane, as shown in Figure 3, the binuclear cations are assembled forming open channels running along the *a* crystallographic axis. These channels, with a diameter about 7.0 Å, accommodate the water molecules and chloride counterions. The solid-state structure is stabilized by hydrogen bonding interaction networks involving the coordinated chlorine anion, water molecules, and C−H groups from the crown thioether.

UV/visible Spectroscopy. The electronic spectra of all the complexes have the characteristic pattern shown by Ru^{II}−polypyridyl complexes (Table 2). Each spectrum displays two sets of bands: ligand-centered (LC) $\pi\rightarrow\pi^*$ electronic transitions between 195 and 215 nm and between 300 and 400 nm are observed,[12,13] while the bands appearing in the visible region can be attributed to Ru(d)→L(π^*) metal-to-ligand charge transfer (MLCT).[21]

The UV/vis data for these new complexes can be compared to previously reported systems that involve [Ru(bpy)$_2$]$^{2+}$ and [Ru(NH$_3$)$_4$]$^{2+}$ metal centers (Scheme 2).

For example, the complexes **5**$^{4+}$ and **6**$^{4+}$ also contain the bridging ligand bptz.[22,23] As the metal center bridged by the ligand changes from {Ru(bpy)$_2$}$^{2+}$, through {RuCl([9]-aneS$_3$)}$^+$, to {Ru(NH$_3$)$_4$}$^{2+}$, the MLCT band moves to a longer wavelength (λ_{max} (MLCT) = 683, 751, and 850 nm for complexes **5**$^{4+}$, **1**$^{2+}$, and **6**$^{4+}$, respectively). A similar, but less pronounced, trend[24,25] is observed in the MLCT band for complexes bridged by dpp such as **7**$^{4+}$ and **8**$^{4+}$, with λ_{max}-(MLCT) = 525, 539, and 558 nm for **7**$^{4+}$, **2**$^{2+}$, and **8**$^{4+}$ respectively. However, the trend for **3**$^{2+}$ and related bpym-bridged systems **9**$^{4+}$ and **10**$^{4+}$ is not so clear-cut[26,27] as λ_{max}(MLCT) values are 588, 606, and 697 nm for **3**$^{2+}$, **9**$^{4+}$, and **10**$^{4+}$, respectively. Assuming that the bridging ligand LUMO is approximately the same in energy in complexes containing the same bridge, the UV/vis spectroscopy results

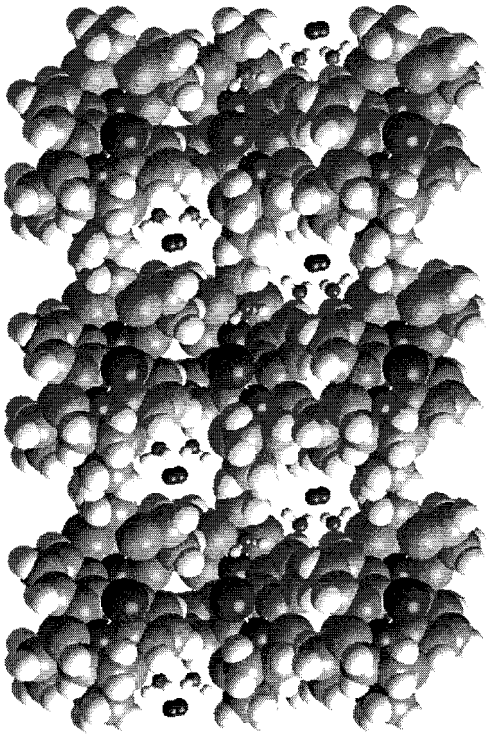

Figure 3. View perpendicular to the crystallographic plane [011] of the crystal packing diagram of [**3**][Cl$_2$] showing open channels formed by complex cations (ball mode) that accommodate the chloride anions and water molecules (ball-and-stick mode.

Table 2. UV/vis Data of Some Bimetallic Complexes with [RuCl([9]aneS$_3$)]$^+$ End Groups in Acetonitrile[a]

complex	λ_{max} (nm)	e (M^{-1} cm^{-1})/1000[a]	assignment
1^{2+}	302	34.9	$\pi-\pi^*$
	751	22.8	MLCT
2^{2+}	270(sh)		$\pi-\pi^*$
	325	34.4	$\pi-\pi^*$
	539	18.7	MLCT
3^{2+}	200	50	$\pi-\pi^*$
	242	22.7	$\pi-\pi^*$
	388	10.1	$\pi-\pi^*$
	545(sh)		
	588	4.3	MLCT

[a] It should be noted that in our preliminary report on the properties of **1**$^{2+}$, all the quoted extinction coefficients were 10 times lower than the correct values, shown in Table 1.

(17) Beech, J.; Cragg, P. J.; Drew, M. G. B. *J. Chem. Soc., Dalton Trans.* **1994**, 719.
(18) Glass, R. S.; Wilson, G. S.; Setzer, W. N. *J. Am. Chem. Soc.* **1980**, *102*, 5068.
(19) Fletcher, N. C.; Junk, P. C.; Reitsma, D. A.; Keene, F. R. *J. Chem. Soc., Dalton Trans.* **1998**, 133.
(20) Schoberl, U.; Magnera, T. F.; Harrison, R. M.; Fleischer, F.; Pflug, J. L.; Schwab, P. F. H.; Meng, X.; Lipiak, D.; Noll, B. C.; Allured, V. S.; Rudalevige, T.; Lee, S.; Michl, J. *J. Am. Chem. Soc.* **1997**, *119*, 3907.
(21) Haga, M.; Dodsworth, E. S.; Lever, A. B. P. *Inorg. Chem.* **1986**, *25*, 447.
(22) (a) Johnson, J. E. B.; de Groff, C.; Ruminski, R. R. *Inorg. Chem. Acta* **1991**, *187*, 73. (b) Poppe, J.; Moscherosch, M.; Kaim, W. *Inorg. Chem.* **1993**, *327*, 2640.
(23) (a) Ernst, S.; Ksack, V.; Kaim, W. *Inorg. Chem.* **1988**, *27*, 1146. (b) Kaim, W.; Ernst, S.; Ksack, V. *J. Am. Chem. Soc.* **1990**, *112*, 173.
(24) Braunstein, C. H.; Baker, A. D.; Strekas, T. C.; Gafney, H. D. *Inorg. Chem.* **1984**, *23*, 857.
(25) Ruminski, R. R.; Cockroft, T.; Shoup, M. *Inorg. Chem.* **1988**, *27*, 4026.
(26) Rillema, D. P.; Mack, K. B. *Inorg. Chem.* **1982**, *21*, 3849.
(27) Ruminski, R. R.; Peterson, J. D. *Inorg. Chem.* **1982**, *21*, 3706.

Scheme 1. Structure of Thiacrown Complexes Discussed

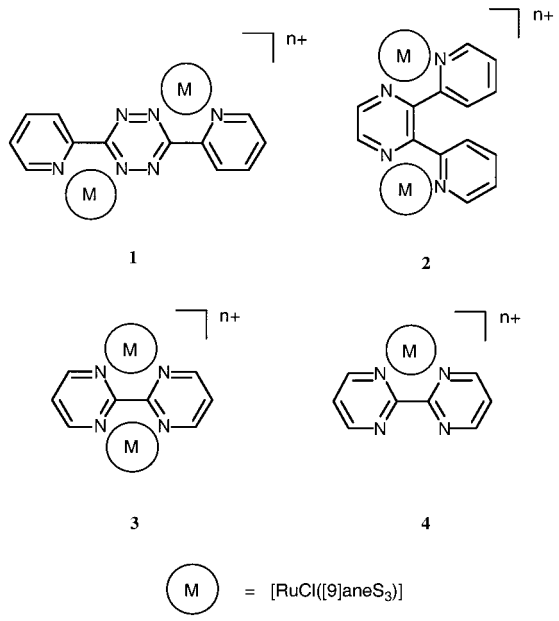

Scheme 2. Previously Reported Ru^{II} Structures Incorporating $\{Ru(bpy)_2\}^{2+}$ and $\{Ru(NH_3)_4\}^{2+}$ Metal Centers

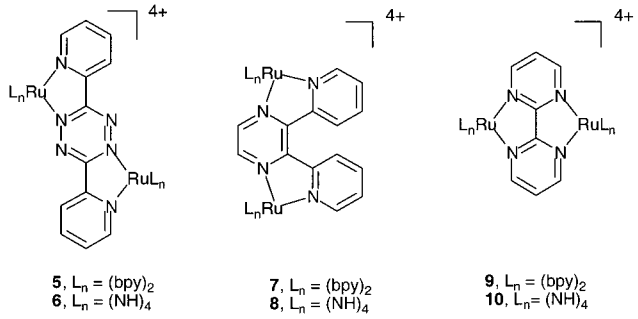

suggest that, despite incorporating a π-donor chloride ligand, the energy of the Ru(II) HOMO in $[RuCl([9]aneS_3)]^+$ is closer to that of the HOMO in a $[Ru(bpy)_2]^{2+}$ fragment than that in $[Ru(NH_3)_4]^{2+}$. This observation is consistent with the appreciable π-acceptor properties of thiacrown ligands, which facilitate d-back-donation from the metal center to the thioether macrocycle.

Electrochemistry. An assessment of ligand bridge mediated intermetallic interactions was carried out using cyclic voltammetry. As well as ligand reductions, each complex displays electrochemically reversible $Ru^{III/II}$ oxidative couples (Table 3). For **1** and **2**, $\Delta E_{1/2}$ was sufficiently large for two distinct, one-electron oxidations to be observed. The cyclic voltammogram (CV) for $\mathbf{3}^{2+}$, shows two oxidations partially obscuring each other. However, both couples are clearly resolved by deconvolution[28] of the data.

Again, the values obtained for the new complexes can be compared with those of analogous systems previously reported in the literature.[22−27]

The first oxidation, $E_{1/2}(1)$, for $\mathbf{1}^{2+}$ is observed at 1.36 V, intermediate to the values observed for $\mathbf{5}^{4+}$ (1.52V) and $\mathbf{6}^{4+}$ (0.69V). Furthermore, $\mathbf{1}^{2+}$ displays an electrochemical interaction of $\Delta E_{1/2} = 0.48$ V, resulting in a comproportionation constant, K_c, of 1.4×10^8. This value is of the same order as that of the bpy complex $\mathbf{6}^{4+}$ ($K_c = 3 \times 10^8$) but much less than the value found for the ammine complex $\mathbf{5}^{4+}$ ($K_c = 10^{15}$). Both of these observations offer further proof of the π-acceptor ability of thioether ligands.

Table 3. Electrochemical Data (mV) for Some Bimetallic Complexes with $[RuCl([9]aneS_3)]^+$ End Groups[a]

	oxidations				reductions
	$E_{1/2}(1)$[b]	$E_{1/2}(2)$	$\Delta E_{1/2}$	K_c[c]	$E_{1/2}(1)$
1	1360	1840	480	1.4×10^8	−49
2	1280	1435	155	4×10^2	−760
					−1230[d]
3	1080	1198	118	100	−903
					−1555[e]

[a] Conditions: vs Ag/AgCl, CH_3CN (HPLC), 0.1 M t-NBu_4 PF_6, under N_2. [b] Unless otherwise stated, couples were electrochemically reversible with $|I_{pc}/I_{pa}| = 1$ and $\Delta E_p < 80$ mV. [c] K_c values were calculated using $\log K_c = [\Delta E_{1/2}/0.059]$. [d] Electrochemically irreversible couple. [e] Deconvolution studies indicate overlap of a reversible and an electrochemically irreversible couple.

For $\mathbf{2}^{2+}$, $E_{1/2}(1)$ is also intermediate between the values observed for the analogous $\mathbf{7}^{4+}$ and $\mathbf{8}^{4+}$. Additionally, $\Delta E_{1/2}$ for $\mathbf{2}^{2+}$, while appreciable ($\Delta E_{1/2} = 155$ mV, $K_c = 425$), is lower than that reported for both of the previously synthesized systems ($\Delta E_{1/2}$ for $\mathbf{7}^{4+} = 190$ mV, $\Delta E_{1/2}$ for $\mathbf{8}^{4+} = 390$ mV).

A comparison of $\mathbf{3}^{2+}$ with $\mathbf{9}^{4+}$ and $\mathbf{10}^{4+}$ shows a similar trend to $\mathbf{2}^{2+}$, with $E_{1/2}(1)$ for $\mathbf{3}^{2+/3+}$ being intermediate between the values observed for $\mathbf{9}^{4+/5+}$ and $\mathbf{10}^{4+/5+}$ and a relatively small peak separation between the two electrochemically reversible oxidation couples: $\Delta E_{1/2} = 118$ mV compared to 160 mV for $\mathbf{9}^{4+}$ and 190 mV in water[27] or 300 mV in dry acetonitrile[29] for $\mathbf{10}^{4+}$. Such a separation results in a K_c for $\mathbf{3}^{3+}$ of 100. These data suggest that both $\mathbf{2}^{2+}$ and $\mathbf{3}^{2+}$ are Robin and Day Class II systems. However, previous studies have indicated that electrochemical data alone do not reveal the complete nature of intermetallic interactions within such systems. More definitive information on such processes can be revealed by the optical properties of the mixed valence state. Since all three new bimetallic complexes display large $\Delta E_{1/2}$, electrochemical generation of their mixed valence state is relatively facile. Consequently, the physical properties of $\mathbf{1}^{3+}$, $\mathbf{2}^{3+}$, and $\mathbf{3}^{3+}$ and the radical cations $\mathbf{1}^+$, $\mathbf{2}^+$, and $\mathbf{3}^+$ were studied via simultaneous electrochemistry and EPR (SEEPR) and spectroelectrochemistry.

EPR. $\mathbf{1}^{3+}$, $\mathbf{2}^{3+}$, and $\mathbf{3}^{3+}$ proved to be EPR silent at room temperature and 77 K. However, isotropic solution spectra were observed for the radical cations $\mathbf{1}^+$, $\mathbf{2}^+$, and $\mathbf{3}^+$.

$\mathbf{2}^+$ and $\mathbf{3}^+$ display broad, featureless spectra, usually observed for Ru^{II} polyazine complexes, centered at $g = 2.0076$ (line width = 21 G) and 2.001 (line width = 13 G), respectively. However, the spectrum of $\mathbf{1}^+$ was well resolved showing good agreement to a simulated model (Figure 4). The observed splitting, due to hyperfine coupling to spin-active nitrogen nuclei, confirms that the LUMO is located

(28) Bard, A. J.; Faulkner, L. R. *Electrochemical Methods. Fundamentals and Applications*; John Wiley and Sons: New York, 1980; pp 236−241.

(29) Baumann, F.; Kaim, W.; Posse, M. G.; Katz, N. E. *Inorg. Chem.* **1998**, *37*, 658.

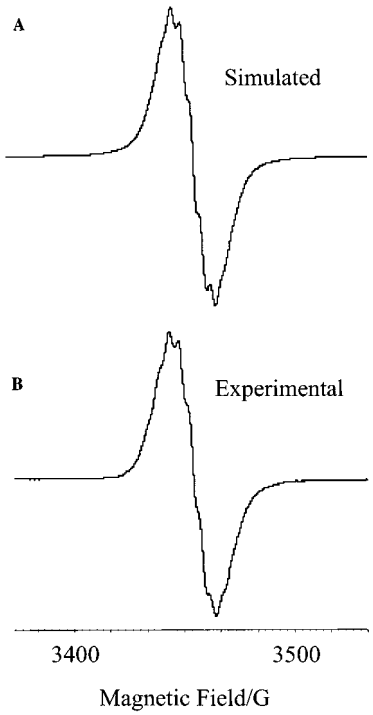

Figure 4. EPR spectrum of $\mathbf{1}^{+}$. A, simulated spectrum; B, experimental spectrum.

on the tetrazine bridge of $\mathbf{1}^{+}$. These data can be compared to those obtained for the previously reported $\mathbf{5}^{3+}$, which also displays a well resolved spectrum at ambient temperatures.[30] The single ^{14}N hyperfine coupling constant ($a^{N} = 5.4$ G) derived from the spectrum and simulation of $\mathbf{1}^{+}$ is in good agreement with the results obtained for $\mathbf{5}^{3+}$ ($a^{N} = 5.5$ G), confirming a convergent p spin population for the coordinated and noncoordinated tetrazine nitrogens. However, unlike $\mathbf{5}^{3+}$, the g value for $\mathbf{1}^{+}$ is higher than that of the free electron ($g = 2.0023$), indicating that, in this case, the singly occupied MO of $\mathbf{1}^{+}$ is close to another, occupied molecular orbital.[31]

Spectroelectrochemistry. Using an OTTLE cell,[32] we carried out spectroelectrochemical studies on all three bimetallic complexes at 240 K. Monoreduction of all three complexes was found to be reversible and accompanied by characteristic optical changes. For example, the $\mathbf{1}^{2+/+}$ couple was monitored via UV/vis spectroscopy, and several well-defined isosbestic points were observed during this process (Figure 5).

During the reduction process, the lowest energy band shifts hypsochromically and becomes much less intense. Such behavior is consistent with that observed for other MLCT bands. The lowest energy bands for $\mathbf{2}^{2+/+}$ and $\mathbf{3}^{2+/+}$ couples also show hypsochromic shifts, but the intensity of these bands shows very little modulation. Again, several isosbestic points are observed for each couple. UV/vis data for the monoreduced products $\mathbf{1}^{+}$, $\mathbf{2}^{+}$, and $\mathbf{3}^{+}$ are summarized in Table 4.

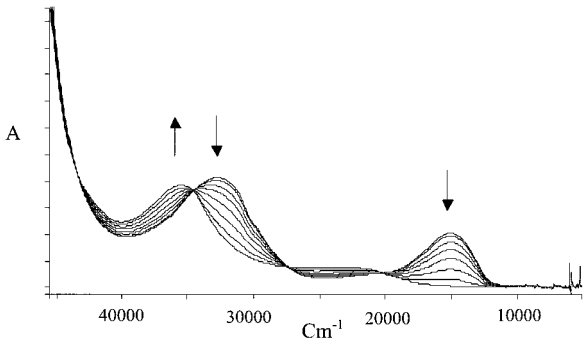

Figure 5. OTTLE plot for the $\mathbf{1}^{2+} \rightarrow \mathbf{1}^{+}$.

Table 4. UV/vis Data for Complex $\mathbf{1}^{+}$, $\mathbf{2}^{+}$, and $\mathbf{3}^{+}$ in Acetonitrile

complex	$\bar{\nu}_{max}$ (cm^{-1})	e (M^{-1} cm^{-1})/1000	assignment
$\mathbf{1}^{+}$	31060	48.2	$\pi-\pi^*$
	26740(sh)		MLCT
	21390	20.2	MLCT
$\mathbf{2}^{+}$	37970	28.7	$\pi-\pi^*$
	31250	20.9	$\pi-\pi^*$
	23561	26.2	MLCT
	20780(sh)		MLCT
$\mathbf{3}^{+}$	31058	11.9	$\pi-\pi^*$
	28890(sh)		$\pi-\pi^*$
	25280	5.3	MLCT
	21670	5.1	MLCT

Table 5. UV/vis Data for Complex $\mathbf{1}^{3+}$, $\mathbf{2}^{3+}$, and $\mathbf{3}^{3+}$ in Acetonitrile[a]

complex	$\bar{\nu}_{max}$ (cm^{-1})	e (M^{-1} cm^{-1})/1000[a]	assignment
$\mathbf{1}^{3+}$	32260	31.60	$\pi-\pi^*$
	14800	23.10	MLCT
	5400	5.19	IVCT
$\mathbf{2}^{3+}$	29310	31.16	$\pi-\pi^*$
	20055	12.85	MLCT
	17970(sh)		MLCT
	5975	2.25	IVCT
$\mathbf{3}^{3+}$	24690	9.33	$\pi-\pi^*$
	16950	4.10	MLCT
	14285(sh)		
	7600	0.47	IVCT

[a] It should be noted that in our preliminary report on the properties of $\mathbf{1}^{3+}$, all the quoted extinction coefficients, including the IVCT, were 10 times lower than the correct values, shown in Table 4.

Table 6. UV/vis Data for Complex $\mathbf{1}^{4+}$, $\mathbf{2}^{4+}$, and $\mathbf{3}^{4+}$ in Acetonitrile

complex	$\bar{\nu}_{max}$ (cm^{-1})	e (M^{-1} cm^{-1})/1000	assignment
$\mathbf{1}^{4+}$	35000(sh)		$\pi-\pi^*$
	32050	20.36	$\pi-\pi^*$
	16000	10.98	MLCT?
$\mathbf{2}^{4+}$	38000(sh)		$\pi-\pi^*$
	29115	27.42	$\pi-\pi^*$
	22500	9.35	MLCT?
	17350(sh)		LMCT?
$\mathbf{3}^{4+}$	24390	7.64	$\pi-\pi^*$
	19050	6.40	MLCT?
	14705(sh)		LMCT?

Each complex was also oxidized in two one-electron steps, and again, these couples were monitored by UV/vis spectroelectrochemistry. All these processes proved to be completely reversible with several isosbestic points being observed (Tables 5 and 6).

One-electron oxidation of $\mathbf{1}^{2+}$ results in the expected hypsochromic shift in the MLCT and also the growth of a low-energy band at 5390 cm^{-1} (Figure 6). The band collapses during the $\mathbf{1}^{3+/4+}$ oxidation process, indicating that this is the expected intervalence charge transfer band, IVCT.

(30) Kaim, W.; Ernst, S.; Kohlmann, S.; Welkerling, P. *Chem. Phys. Lett.* **1985**, *118*, 431.
(31) Yersin, H.; Gallhuber, E. *J. Am. Chem. Soc.* **1984**, *106*, 6582.
(32) McWhinnie, S. L.; Charsley, S. M.; Jones, C. J.; McCleverty, J. A.; Yellowlees, L. J. *J. Chem. Soc., Dalton Trans.* **1993**, 413.

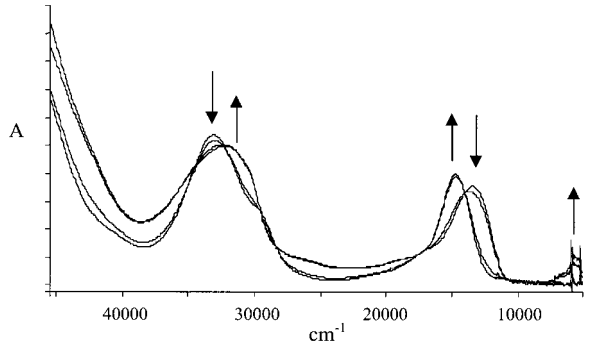

Figure 6. OTTLE plot for the $\mathbf{1}^{2+} \rightarrow \mathbf{1}^{3+}$.

It should be noted that the only other report of an IVCT transition in a $Ru^{III/II}$ complex incorporating the bptz bridging ligand involved $\mathbf{6}^{5+}$. However, in this case, despite a very large K_c value (10^{15}), a low-intensity ($e = 500\ M^{-1}\ cm^{-1}$) IVCT at 1450 nm, 6896 cm^{-1}, was observed.[22b] The low intensity of the transition is attributable to the d_p metal orbitals being directed toward the center of the a-dimine chelate system as opposed to being linearly orientated toward each other. In contrast to these observations, the IVCT for $\mathbf{1}^{3+}$ is an order of magnitude more intense, with $e = 5000\ M^{-1}\ cm^{-1}$.

Application of the Hush theory[5c] to the IVCT data of $\mathbf{1}^{3+}$ yields a bandwidth at half-height, $\Delta\nu_{1/2}$, which is much wider than the experimental value; $\Delta\nu_{1/2} = (2310\nu)^{1/2}\ cm^{-1}$, $\Delta\nu_{1/2}$ ($\mathbf{1}^{3+}$, calcd) = 3530 cm^{-1}, $\Delta\nu_{1/2}$ ($\mathbf{1}^{3+}$, exptl) $\approx$ 1375 cm^{-1}. The energy and intensity of the band are consistent with properties previously reported for Class III IVCT. In fact, the bandwidth is exceptionally narrow for such an intense IVCT indicating intense resonance coupling. Accordingly, the degree of electronic coupling, H_{AB}, can be estimated to approximately $\upsilon_{max}/2 = 2688\ cm^{-1}$. Indeed, the properties of $\mathbf{1}^{3+}$ are somewhat reminiscent of the CT ion itself, which, depending on conditions, has been observed at 6250−6400 cm^{-1}, with $\epsilon = 5000-7620\ M^{-1}\ cm^{-1}$.[33]

During the $\mathbf{2}^{2+/3+}$ oxidation, a low-energy band partially obscured by solvent overtones, centered around 5975 cm^{-1}, was generated (Figure 7). Again, this band collapses during the oxidation to $\mathbf{2}^{4+}$. The transition is less intense than the corresponding band for $\mathbf{1}^{3+}$. However, a value of $\epsilon = 2250\ M^{-1}\ cm^{-1}$ is still relatively large, a characteristic that is inconsistent with Hush theory descriptors of Class II behavior. Further evidence suggesting that $\mathbf{2}^{3+}$ exhibits Class III behavior comes from the measurement of $\Delta\nu_{1/2}$. The experimental value of $\Delta\nu_{1/2}$ for $\mathbf{2}^{3+}$ is 1600 cm^{-1}, whereas Hush theory predicts a value of 3715 cm^{-1}. Therefore, H_{AB} can be approximated as $\upsilon_{max}/2 = 2988\ cm^{-1}$.

IVCT have not been reported for $\mathbf{7}^{5+}$ and $\mathbf{8}^{5+}$. Indeed, it is worth noting that, despite its common use as a bridging ligand, as far as we are aware, this is the first IVCT observed in a dpp-bridged $Ru^{III/II}$ system.

(33) (a) Richardson, D. E.; Taube, H. *J. Am. Chem. Soc.* **1983**, *105*, 40. (b) Selaymeh, F.; Berhane, S.; Yusof, R.; de la Rosa, R.; Fung, E. Y.; Matamoros, R.; Lau, K. W.; Zheng, Q.; Kober, E. M.; Curtis, J. C. *Inorg. Chem.* **1993**, *32*, 3895.

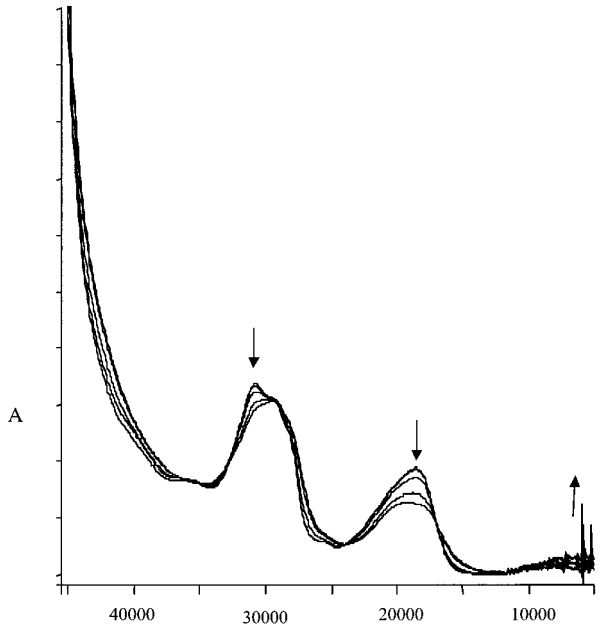

Figure 7. OTTLE plot for the $\mathbf{2}^{2+} \rightarrow \mathbf{2}^{3+}$.

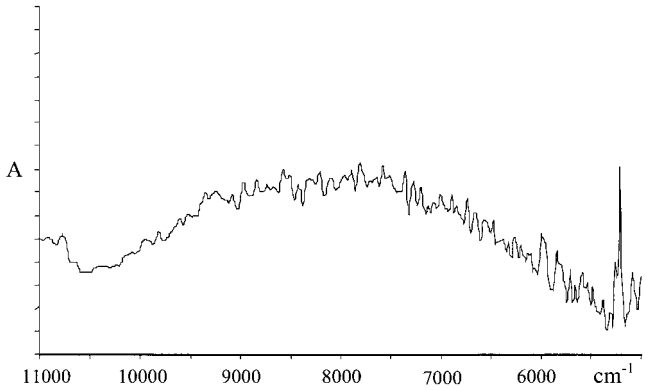

Figure 8. $[\mathbf{3}^{3+} - \mathbf{3}^{2+}]$ difference spectrum for the NIR region.

Unusually, the one-electron oxidation of $\mathbf{3}^{2+}$ results in the growth of a new, relatively intense band seen as a shoulder at 700 nm (14 285 cm^{-1}). This band is not assigned to IVCT as there is a further increase in intensity when $\mathbf{3}^{4+}$ is generated.

However, generation of $\mathbf{3}^{3+}$ appears to be accompanied by the growth of a transition centered around 8000 cm^{-1}, an area of the spectrum largely obscured by solvent overtones. This NIR band is fully revealed by the difference spectrum for $[\mathbf{3}^{3+} - \mathbf{3}^{2+}]$ (Figure 8). The observed transition collapses on oxidation to $\mathbf{3}^{4+}$, behavior that is consistent with a low-intensity IVCT. In contrast, IVCT for $\mathbf{9}^{5+}$ and $\mathbf{10}^{5+}$ were not observed.[26,27]

The experimental $\Delta\nu_{1/2}$ value for this transition, ~4600 cm^{-1}, is in good agreement with the Hush theory prediction of 4300 cm^{-1}. This observation, the low intensity of the transition ($\epsilon < 10^3\ M^{-1}\ cm^{-1}$), and the relatively small value of K_c are all indicative of a valence-trapped Class II system.[5e] Consequently, H_{AB} can be obtained by eq 1:[5]

$$H_{AB} = \frac{2.06 \times 10^{-2}}{R}(\nu_{max}\epsilon_{max}\nu_{1/2})^{1/2} \qquad (1)$$

where R is the transition dipole length, approximated by the intermetallic distance of 5.705 Å obtained from the crystallographic data. This leads to an H_{AB} of 470 cm^{-1}, a value that is comparable to several pyrazine-bridged CT ion analogues.[5d,5e]

Discussion and Conclusion

[Ru(DMSO)Cl$_2$([9]aneS$_3$)] has proved to be an excellent starting material for the synthesis of ligand-bridged bimetallic complexes incorporating [RuCl([9]aneS$_3$)]$^+$ metal centers. While K_c values for the Ru$^{III/II}$ mixed valence states of these new complexes are lower than those obtained for N-donor systems, application of Hush theory to the optical properties of **1**$^{3+}$, **2**$^{3+}$, and **3**$^{3+}$ clearly indicates strong metal coupling. Indeed, a comparison of the optical properties of **6**$^{5+}$ and **1**$^{3+}$ indicates that metal coupling in the latter complex is more intense than the analogous [(NH3)$_4$Ru]$^{2+}$ system.

Despite several reports to the contrary,[22b,32] it is often assumed that K_c is a measure of metal−metal coupling. In fact, its magnitude is determined by several factors. The anomalously low values of K_c for **1**$^{3+}$, **2**$^{3+}$, and **3**$^{3+}$ may require a consideration of the various terms that contribute to ΔG_c, the free energy of comproportionation:[5e,34]

$$\Delta G_c = \Delta G_r + \Delta G_e + \Delta G_s + \Delta G_i \qquad (2)$$

where ΔG_r is the free energy of resonance, ΔG_e is an electrostatic term that takes into account the mutual repulsion of the two cationic metal centers, ΔG_s is an entropic factor that takes the value (1/2)RT ln 1/4, and ΔG_i is a synergistic effect due to the stabilization of Ru(II) by Ru(III) or vice versa. Only ΔG_r is a measure of true metal−metal electronic coupling.[34a]

It is known that ΔG_e can make a significant contribution to ΔG_c, particularly in nonaqueous solvents.[34b] Furthermore, a study of the oxidation and reduction couples of ligand-bridged diiron complexes has demonstrated that ΔG_e is dependent on the size of the charge of the system studied.[34c] Consequently, K_c is larger for more highly charged species. From these arguments, it seems likely that ΔG_e for [{RuCl([9]aneS$_3$)}$_2$(m−L)]$^{n+}$ will be less than that for more highly charged [{(NH$_3$)$_n$Ru}$_2$(m−L)]$^{n+}$ and [{(diimine)$_n$Ru}$_2$(m−L)]$^{n+}$ systems. The experimental values of K_c for **1**$^{3+}$, **2**$^{3+}$, and **3**$^{3+}$ do seem to support this hypothesis. Furthermore, anomalous values of K_c have also been observed for other highly interacting d^5/d^6 systems such as **11**[35] and **12**[36] (Scheme 3) that are similarly expected to have low ΔG_e values. However, it should be noted that, while there are examples of low-charged mixed valence systems with large K_c values, many such systems display more complex

Scheme 3. Selected Low-Charged Mixed Valence Systems Incorporating π-Acceptor and π-Donor Ligands

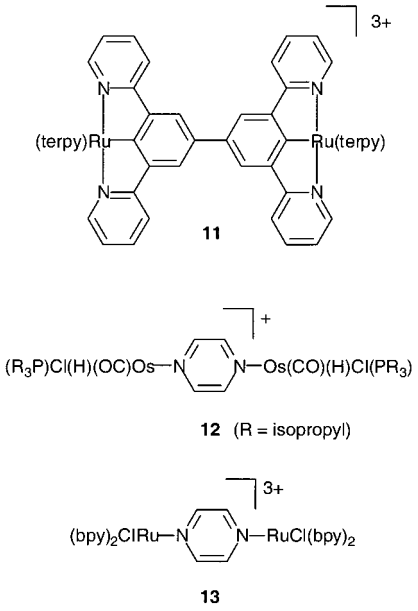

interactions such as direct metal−metal interactions,[37] or electronic contributions from ligand-centered radical structures.[38]

Although electrostatic interactions within [{RuCl([9]aneS$_3$)}$_2$(m−L)]$^{n+}$ appear to be reduced, the comparison between **1**$^{3+}$ and analogous N-donor systems demonstrates that ΔG_r has also been enhanced. However, the combination of π-acceptor and π-donor within the [RuCl([9]aneS$_3$)]$^+$ unit could also favor the mixed valence state by stabilizing both Ru^{II} and Ru^{III} oxidation states, thus leading to a consequent enhancement of ΔG_i. Again, it should be noted that **11** and **12** also incorporate π-acceptor and π-donor ligands. Nevertheless, there are several examples of low-charged systems incorporating π-acceptor and π-donor ligands that show low resonance energies, for example, **13**.[39] It may be that, in these cases, the π-acceptor ligands back-bond too efficiently for electron density to become delocalized over the bridging ligand: bipyridyl ligands are strong π-acids, with back-bonding occurring via ligand π*-orbitals, while back-bonding in [9]-ane-S$_3$ only occurs through those C−S σ*-orbitals that are in-plane with the metal t$_{2g}$ set.[40] Clearly, a definitive answer to the apparent enhanced resonance interaction will require an investigation of the molecular orbitals and delocalization pathways available within [RuCl([9]aneS$_3$)]$^+$-based systems.

Further synthetic studies will probe the nature of the metal−metal interaction and explore the use of related metal

(34) (a) Sutton, J. E.; Taube, H. *Inorg. Chem.* **1981**, *20*, 3125. (b) Rezvani, A. R.; Bensimon, C.; Cromp, B.; Reber, C.; Greedan, J. E.; Kondratiev, V. V.; Crutchley, R. J. *Inorg. Chem.* **1997**, *36*, 3322. (c) Ferrere, S.; Elliott, C. M.; *Inorg. Chem.* **1995**, *34*, 5818.
(35) (a) Beley, M.; Collin, J.-P.; Louis, R.; Metz, B.; Sauvage, J.-P. *J. Am. Chem. Soc.* **1991**, *113*, 8521. (b) Patoux, C.; Launay, J.-P.; Beley, M.; Chodorowski-Kimmes, S.; Collin, J.-P.; Stuart, S.; Sauvage, J.-P. *J. Am. Chem. Soc.* **1998**, *120*, 3717.
(36) Glöckle, M.; Kaim, W.; Fielder, J. *Organometallics* **1998**, *17*, 4923.
(37) (a) Bardwell, D.; Jeffery, J. C.; Joulié, L.; Ward, M. D. J. *Chem. Soc. Dalton Trans.* **1993**, 2255. (b) Bardwell, D.; Horsburgh, L.; Jeffery, J. C.; Joulié, L.; Ward, M. D.; Webster, E.; Yellowlees, L. J. *J. Chem. Soc., Dalton Trans.* **1996**, 2527.
(38) Kaim, W.; Kasak, V.; Binder, H.; Roth, E.; Jordanov, J. *Angew. Chem., Int. Ed. Engl.* **1988**, *27*, 1174.
(39) Callahan, R. W.; Keene, F. R.; Meyer, T. J.; Salmon, D. J. *J. Am. Chem. Soc.* **1977**, *99*, 1064.
(40) (a) Mullen, G. E. D.; Went, M. J.; Wocaldo, S.; Powell, A. K.; Blower, P. J. *Angew. Chem., Int. Ed. Engl.* **1997**, *36*, 1205. (b) Mullen, G. E. D.; Fässler, T. F.; Went, M. J.; Howland, K.; Stein, B.; Blower, P. J. *J. Chem. Soc., Dalton Trans.* **1999**, 3759.

centers and new bridging ligands to produce structures with possible applications as devices.

Experimental Section.

Materials and Procedures. The complex [Ru(DMSO)Cl_2([9]-aneS_3)][14] and ligand bptz[15] was prepared according to previously published procedures. All other reagents were obtained commercially and used as supplied. All reactions were conducted under an atmosphere of nitrogen. Products were dried at room temperature in a vacuum desiccator for ca. 10 h prior to characterization.

Physical Measurements. ^{1}H NMR spectra were recorded on a Bruker AM250 machine working in Fourier transform mode. ^{1}H NMR spectra were acquired in a range of 1−12 ppm with 32 K data points, and coupling constants are given in hertz. Mass spectral data was collected on a Micromass Prospec spectrometer operating in positive ion fast atom bombardment mode (FAB+) with a NOBA matrix. UV/vis spectra were recorded on a Unicam UV/vis spectrometer UV2. Elemental analyses were obtained using a Perkin-Elmer 2400 analyzer working at 975 °C. Cyclic voltammetric measurements were carried out using an EG&G 253 potentiostat controlled by 270 Electrochemical Research Software. A three-electrode cell was used with an Ag^+/AgCl reference electrode separated from a Pt disk working electrode and Pt wire auxiliary electrode. 0.1 M^{-1} dm^3 tetra-*n*-butylammonium hexafluorophosphate in acetonitrile, doubly recrystallized from ethyl acetate/diethyl ether, was used as a support electrolyte. A scan rate of 200 mV/s was employed. Procedures and instrumentation for spectroelectrochemical studies have been described elsewhere.[32]

Syntheses: [1](PF$_6$)$_2$. To a solution of 0.215 g (0.5 mmol) of [Ru(DMSO)Cl_2([9]aneS_3)] in 20 mL of 1:1 ethanol/water was added 3,6-bis(2-pyridyl)1,2,4,5-tetrazine (59 mg, 0.5 equiv) and the reaction mixture refluxed for 3 h. After the mixture was filtered, NH_4PF_6 (122.5 mg, 3 equiv) was added, resulting in the precipitation of a crude product. Column chromatography (grade V alumina), eluting with acetonitrile/toluene (1:1), gave 139.1 mg of bimetallic complex **1** (48 %) as a blue powder. ^{1}H NMR, major isomer: δ 2.70−3.65 (m, 24H), 7.95−8.05 (m, 2H), 8.35−8.45 (m, 2H), 8.89 (dq, J = 7.93 and 0.90, 2H), 9.33 (dq, J = 6.10 and 0.90, 2H). MS *m*/*z* (%): 1016 (15) [$M^+ + PF_6$], 871 (30) [$M^+ - H^+$]. Anal. Calcd for $C_{24}H_{32}Cl_2F_{12}N_6P_2Ru_2S_6 \cdot 4H_2O$: C, 23.39; H, 3.285; N, 6.82. Found: C, 23.49; H, 3.06; N, 6.74.

[2](PF$_6$)$_2$. To a solution of 0.215 g (0.5 mmol) of [Ru(DMSO)-Cl_2([9]aneS_3)] in 20 mL of 1:1 ethanol/water was added 2,3-bis-(2-pyridyl)pyrazine (58.5 mg, 0.5 equiv) and the reaction mixture refluxed for 3 h. After the mixture was filtered, NH_4PF_6 (122.5 mg, 3 equiv) was added, resulting in the precipitation of a crude product. Column chromatography (grade II alumina), eluting with acetonitrile, gave 142 mg of **2** (49%) as a purple powder. ^{1}H NMR, major isomer: δ 2.30−3.20 (m, 24H), 7.66 (m, 2H), 7.85 (dd, J = 8.23 and 1.53, 2H), 8.56 (d, J = 8.23, 2H), 8.80 (s, 2H), 9.22 (d, J = 4.90, 2H). MS *m*/*z* (%): 1014 (35) [$M^+ + PF_6$], 868 (35) [$M^+ - H^+$]. Anal. Calcd for $C_{26}H_{34}Cl_2F_{12}N_4P_2Ru_2S_6 \cdot H_2O$: C, 26.55; H, 3.09; N, 4.76. Found: C, 26.26; H, 3.28; N, 4.89.

[3](PF$_6$)$_2$. To a solution of 0.215 g (0.5 mmol) of [Ru(DMSO)-Cl_2([9]aneS_3)] in 20 mL of 1:1 ethanol/water was added 2,2′-bipyrimidine (39.5 mg, 0.5 equiv), and the reaction mixture was left to reflux for 3 h. After the mixture was filtered, NH_4PF_6 (122.5 mg, 3 equiv) was added, resulting in the precipitation of a crude product. The product was reprecipitated from acetonitrile/diethyl ether. Yield: 106.1 mg of **3** (39%) as a black powder. ^{1}H NMR, major isomer (CD_3CN): δ 2.50−3.10 (m, 24H), 9.227 (d, 4H, J = 5.7), 7.798 (t, 2H, J = 5.7). MS *m*/*z* (%): 935 (35) [$M^+ + PF_6$], 791 (30) [$M^+ - H^+$]. Anal. Calcd for $C_{20}H_{30}Cl_2F_{12}N_4P_2Ru_2S_6 \cdot 1.5H_2O$: C, 21.66; H, 3.04; N, 5.05. Found: C, 21.67; H, 3.02; N, 4.77.

Table 7. Crystallographic Data for [{Ru([9]aneS_3)Cl}$_2$(bpym)]$Cl_2 \cdot 4H_2O$ **3**

formula	$C_{20}H_{38}Cl_4N_4O_4Ru_2S_6$
M	934.84
cryst syst	monoclinic
space group	$P2_1/a$
a, Å	10.929(14)
b, Å	13.514(17)
c, Å	11.299(16)
β, deg	90.52(1)
V, Å^3	1669
Z	2
D_{calcd}, g/cm^3	1.557
μ, mm^{-1}	1.636
F(000)	940
final *R* indices [$I > 2\sigma(I)$]	
R_1 and wR_2[a]	0.0781, 0.1879
R indices (all data)	
R_1 and wR_2	0.1296, 0.2139

[a] $R_1 = \sum||F_o| - |F_c||/\sum|F_o|$, $wR2 = \{\sum[w(F_o^2 - F_c^2)^2]/\sum[w(F_o^2)^2]\}^{1/2}$, $w = 1/[\sigma^2(F_o^2) + (0.145P)^2 + 2.84P]$, where $P = [2F_c^2 + \max(F_o^2, 0)]/3$.

Crystallography. The chloride salt of $\mathbf{3}^{2+}$ could be obtained via metathesis of acetone solutions of [**3**](PF$_6$)$_2$ with [(NBu$_4$)Cl]. Single crystals of [**3**]Cl_2 were obtained by slow evaporation from an acetonitrile solution of the complex at room temperature. The crystal data and refinement details are given in Table 7.

X-ray data were measured using the MAR research image plate system using graphite-monochromated Mo Kα radiation (λ = 0.71073 Å) at ∼295 K. The selected crystal mounted in a glass capillary under a saturated solvent atmosphere was positioned 70 mm from the plate. Frames (95) were taken at 2° intervals using a counting time adequate for the crystal diffraction pattern. Data analysis was performed with the XDS program.[41] an empirical absorption correction was applied to intensities of **1a**, using version of the DIFABS program modified for image plate geometry.[42]

Intensities of 4970 observations were collected, of which 3040 were independent reflections giving an R_{int} of 0.1057. The structure was solved by direct methods and subsequent difference Fourier syntheses and refined by the full-matrix least-squares refinement method on F^2 using the SHELX97 software package.[43] The successful refinement was obtained assuming a twinned crystal. The instruction TWIN 1 0 0 0 1 0 0 0 −1 2 was used together with the BASF parameter refined to 0.44(2). Anisotropic displacements were refined for all non-hydrogen atoms. Hydrogen atoms bonded to carbon atoms were introduced in the refinement at idealized geometric positions with a $U_{iso} = 1.2 \times U_{eq}$ of the parent carbon atom. Hydrogen atoms of water molecules were retrieved from difference Fourier maps and introduced into refinement assuming O−H distances and H−O−H angles constrained to 0.85 Å and 109.5°, respectively. The final refinements of 194 parameters converged to R_1 and wR_2 values quoted in Table 7. The final residual electronic density in ΔF map, in the range from 1.27 to −1.33 e/Å^3, was within the expected values. The ORTEP plot was drawn with the PLATON program,[44] while the crystal packing diagram was performed using CERIUS2 software.[45]

(41) Kabsch, W. *J. Appl. Crystallogr.* **1988**, *21*, 916.
(42) Walker, N.; Stuart, D. DIFABS. *Acta Crystallogr. Sect. A* **1983**, *39*, 158.
(43) (a) Sheldrick, G. M. SHELXS-86. *Acta Crystallogr. Sect. A* **1990**, *46*, 467. (b) Sheldrick, G. M. *SHELX-97*; University of Göttingen: Göttingen, Germany, 1997.
(44) Spek, A. L. *PLATON, a Multipurpose Crystallographic Tool*; Utrecht University: Utrecht, The Netherlands, 1999.

Acknowledgment. We are grateful for financial support from the EPSRC (M.G.B.D., L.J., S.R., J.A.T., and L.Y.), the Royal Society (J.A.T.), and FCT (C.A., J.M., V.F., and T.S.) under PRAXIS XXI program (Contract PRAXIS/PCEX/CQUI/122/96). J.M. also acknowledges the FCT for a Ph.D. grant.

(45) *CERIUS2*, version 3.5; Molecular Simulations, Inc.: San Diego, 1997.

Supporting Information Available: CIF file for the structure reported in this paper, listings of bond lengths (Å) and angles (deg) of hydrogen bonds in [**3**]Cl_2, cyclic voltammogram of $\mathbf{3}^{2+}$, deconvolution of oxidation processes in $\mathbf{3}^{2+}$, and an OTTLE plot for the $\mathbf{3}^{2+} \rightarrow \mathbf{3}^{3+} \rightarrow \mathbf{3}^{4+}$. This material is available free of charge via the Internet at http://pubs.acs.org.

IC010882I